

The Large Hadron Collider

Lyndon Evans

CERN – European Organization for Nuclear Research, Geneva, Switzerland

1. INTRODUCTION

The Large Hadron Collider (LHC) at CERN is now in its final installation and commissioning phase. It is a two-ring superconducting proton-proton collider housed in the 27 km tunnel previously constructed for the Large Electron Positron collider (LEP). It is designed to provide proton-proton collisions with unprecedented luminosity ($10^{34}\text{cm}^{-2}\cdot\text{s}^{-1}$) and a centre-of-mass energy of 14 TeV for the study of rare events such as the production of the Higgs particle if it exists. In order to reach the required energy in the existing tunnel, the dipoles must operate at 1.9 K in superfluid helium. In addition to p-p operation, the LHC will be able to collide heavy nuclei (Pb-Pb) with a centre-of-mass energy of 1150 TeV (2.76 TeV/u and 7 TeV per charge). By modifying the existing obsolete antiproton ring (LEAR) into an ion accumulator (LEIR) in which electron cooling is applied, the luminosity can reach $10^{27}\text{cm}^{-2}\cdot\text{s}^{-1}$.

The LHC presents many innovative features and a number of challenges which push the art of safely manipulating intense proton beams to extreme limits. The beams are injected into the LHC from the existing Super Proton Synchrotron (SPS) at an energy of 450 GeV. After the two rings are filled, the machine is ramped to its nominal energy of 7 TeV over about 28 minutes. In order to reach this energy, the dipole field must reach the unprecedented level for accelerator magnets of 8.3 T. This high field can only be achieved using “conventional” and affordable superconducting material (NbTi), by cooling the magnets in superfluid helium at 1.9 K. The cryogenic equipment needed to produce the 100 tons or so of superfluid helium is unprecedented in scale and complexity.

The tunnel diameter in the regular arc is only 3.8 m, insufficient for the installation of two separate rings. The two rings are therefore incorporated into a single magnetic structure with two sets of coils in a common yoke and cryostat.

2. MACHINE PERFORMANCE

At nominal luminosity, the energy stored in each beam is more than 350 MJ (equivalent to 80 kg of TNT). This is more than two orders of magnitude in stored energy, and three orders of magnitude in energy density (due to the very small beam emittance) than in any other previous machine (Figure 1). It imposes unprecedented conditions on the reliability of the safety systems which must abort the beams cleanly if necessary as well as on the collimation systems which protect the machine and detectors from halo particles.

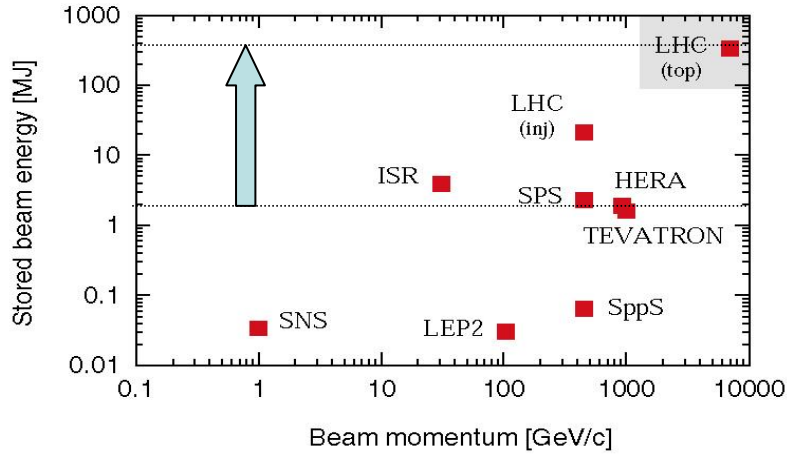


Figure 1: a. Energy stored in the accelerator beam, as a function of beam momentum. At less than 1% of nominal intensity LHC enters new territory.

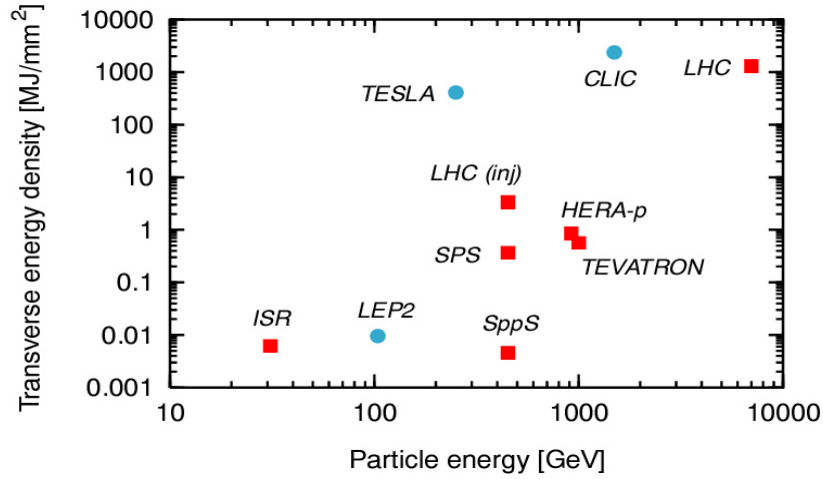


Figure 1: b. Stored energy density as a function of beam momentum. Transverse energy density is a measure of damage potential and is proportional to luminosity.

The number of events per second generated by beam-beam collisions for a given process is given by:

$$N = L\sigma$$

where σ is the cross section for the process in question and L is the luminosity. For the study of very rare events the luminosity must be as high as possible. The luminosity depends only on beam parameters and can be written for a Gaussian beam profile as:

$$L = \frac{N_b^2 n f_r \gamma}{4\pi \varepsilon_n \beta^*}$$

where N_b is the number of particles per bunch, n the number of bunches per beam, f_r the revolution frequency (11.245 kHz), γ the relativistic gamma factor, ε_n the normalized transverse emittance and β^* the beta function at the collision

point. As well as the rare hard collisions between particles, the particles in one beam experience the global electromagnetic field of the other beam (the beam-beam interaction). This force is very nonlinear and gives rise to unwanted effects if not limited to as small a value as possible. Therefore the bunches must have a crossing angle in order to limit the beam-beam force to the colliding bunches. This produces a geometrical luminosity reduction factor F given by:

$$F = 1 / \sqrt{1 + \left(\frac{\theta_c \sigma_z}{2\sigma^*} \right)^2}$$

where θ_c is the full crossing angle at the interaction point (IP), σ_z the rms bunch length and σ^* the transverse rms beam size at the crossing point.

Table 1 shows the main parameters required to reach a peak luminosity of $10^{34} \text{ cm}^{-2} \text{ s}^{-1}$ for proton-proton collisions at 14 TeV centre-of-mass. It can be seen from the table that for the first time in a hadron machine, the synchrotron radiation at top energy is not negligible. At 3.6 kW per beam it is still very small compared with lepton storage rings and has no influence on the design of the radio frequency system, but this power is radiated into a cryogenic environment and strongly influences the design of the vacuum and cryogenic systems.

Table 1: Performance parameters.

• Circumference	26.7	km
• Beam energy at collision	7	TeV
• Beam energy at injection	0.45	TeV
• Dipole field at 7 TeV	8.33	T
• Luminosity	10^{34}	$\text{cm}^{-2} \cdot \text{s}^{-1}$
• Beam current	0.56	A
• Protons per bunch	1.1×10^{11}	
• Number of bunches	2808	
• Nominal bunch spacing	24.95	ns
• Normalized emittance	3.75	μm
• Total crossing angle	300	μrad
• Energy loss per turn	6.7	keV
• Critical synchrotron energy	44.1	eV
• Radiated power per beam	3.8	kW
• Stored energy per beam	350	MJ
• Stored energy in magnets	11	GJ
• Operating temperature	1.9	K

2.1. Machine Layout

The basic layout of the LHC follows the LEP tunnel geometry and is shown in Figure 2. The machine has eight arcs and straight sections. Each straight section is approximately 528 m long. Four of the straight sections house the LHC detectors whilst the other four are used for machine utilities, radio frequency, collimation and beam abort. The two high luminosity detectors are located at diametrically opposite straight sections. The ATLAS detector is located at Point 1 and CMS at Point 5, which also incorporates the small angle scattering experiment TOTEM. Two more detectors are

located at Point 2 (ALICE) and at Point 8 (LHCb), which also contain the injection systems for the two rings. The beams only cross from one ring to the other at these four locations.

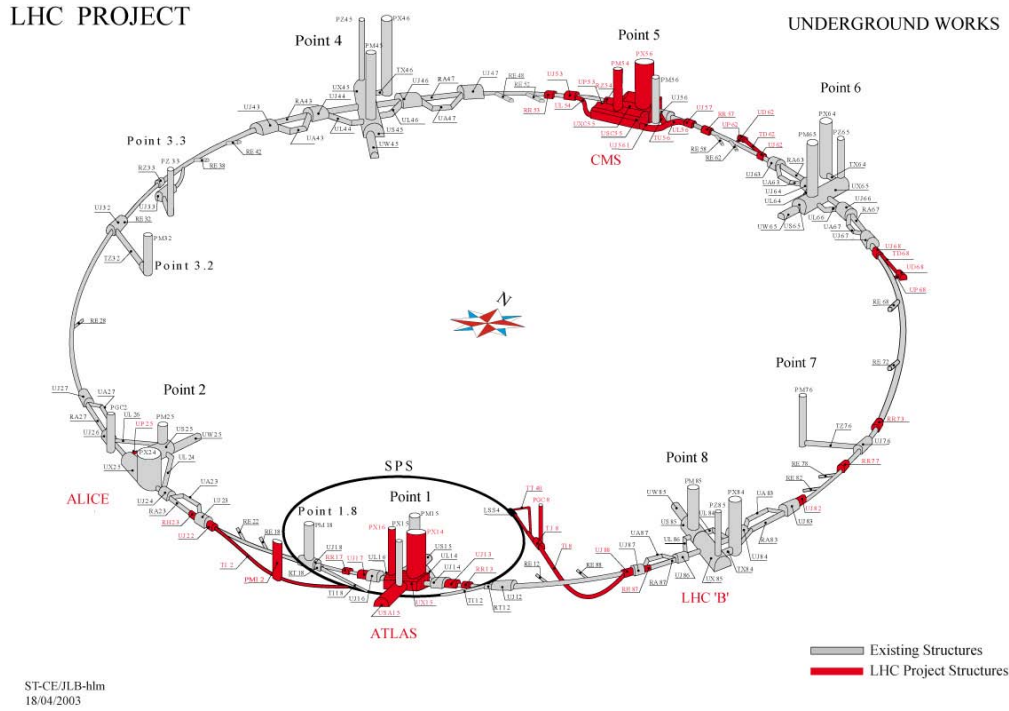


Figure 2: LHC layout.

In order to leave enough space for the LHCb spectrometer magnet in the already existing experimental cavern at Point 8, the interaction point at this location is shifted by 11.25 m towards Point 7. Bunches with the nominal 25nsec separation collide at all four crossing points simultaneously. However, because of this displacement, the only other bunch separation with simultaneous collisions in all four detectors is 75nsec. For early commissioning, this bunch separation is interesting because there is no possibility of electron cloud buildup (see below) and the number of long-range beam-beam interactions is reduced, simplifying early machine operation. The 25 GeV proton synchrotron (the first circular machine in the injector chain), where the LHC bunch structure is generated, has therefore been equipped with the means to provide either of these two bunch spacings.

Straight sections at Points 3 and 7 contain two collimation systems for capturing stray particles. Point 3 is designed to capture off-momentum particles (momentum collimation) and Point 7 for removing the beam halo (betatron collimation). Point 4 contains the two Radio Frequency systems, one independent system for each beam operating at 400 MHz, twice the frequency of the LHC injector. Finally, Point 6 contains the two beam abort systems which will allow the beams to be extracted safely and dumped onto external absorbers.

The regular LHC lattice was designed to maximize the amount of bending power in the arc by making the dipoles as long as reasonably possible. This minimizes the amount of dead space between interconnects as well as the number of dipoles to be manufactured, tested and interconnected. After careful optimization, the dipole length was chosen to be 14.2 m (magnetic), 15 m overall with 23 regular lattice periods per arc. Each period is 106.9 m long and is made up of

six dipoles and two short straight sections each of 6.6 m length containing the main quadrupoles and lattice correctors. The two apertures of ring 1 and ring 2 are separated by 194 mm. Both dipole apertures are connected in series whereas the quadrupoles are powered in two families, all focusing quadrupoles of rings one and two in series and likewise for the defocusing quadrupoles.

The transition from the regular arc contains a dispersion suppressor consisting of two perturbed lattice periods. The purpose of the dispersion suppressor is threefold:

- adapt the LHC reference orbit to the geometry of the tunnel,
- cancel the horizontal dispersion generated in the arc and by the separation and recombination dipoles,
- help with the matching of the beams between the arcs and straight sections.

A generic design of a dispersion suppressor can be made using standard arc cells with missing dipoles and dipoles of different length to those in the arc. However, due to the constraints imposed by the geometry of the existing tunnel and the economy of having only one standard dipole length, the dispersion can only be fully cancelled by individual powering of the quadrupoles in the dispersion suppressor cells. These quadrupoles also provide additional parameters for matching the insertion optics.

The short straight sections in the arcs contain the main quadrupoles and also the correction sextupoles for chromaticity control and the orbit correction dipoles. Depending on their location, they can also contain trim normal or skew quadrupoles or Landau damping octupoles.

The optics of the long straight sections differ according to their functionality. At Points 1 and 5 in the high luminosity insertions the small beta (0.5 m) at the collision point is generated with the help of a quadrupole triplet assembly. At Points 2 and 8, the optics at the 450 GeV injection level must allow beam injection whereas at top field the beams must be focused to a moderate beta. At the utility insertions the optics is tailored to their functionality. Details of the optics in the various insertions can be found elsewhere [1].

2.2. Main Hardware Systems

The main hardware systems include magnets, vacuum, cryogenics, radio frequency, power converters, injection and extraction equipment, beam instrumentation, collimation and controls, far too numerous for an article of this size. Details can be found in the LHC Design Report [1]. Only a few selected systems of general interest will be treated here.

2.3. Magnets

The LHC contains more than 7000 superconducting magnets ranging from the 15 m long main dipoles to the 10 cm long octupole/decapole correctors inside the dipole cold masses as well as more than 100 conventional warm magnets not counting the 500 or so conventional magnets in the two 2.6 km long transfer lines between the SPS and the LHC. The most challenging are the superconducting dipoles and the quadrupoles in the arcs, dispersion suppressor and matching regions.

The three large superconducting accelerators operating today, the Tevatron (FNAL), HERA (DESY) and RHIC (BNL) all use magnets made with classical Nb-Ti superconductor cooled with supercritical helium at a temperature slightly above 4.2 K. In each case, the nominal field is below or around 5 T. In order to increase the field to above 8 T, two possibilities exist today.

Figure 3 shows the critical current density of two superconductors available commercially today. The Nb-Ti conductor at 4.5 K has a critical current density that is too low to reach the LHC objective. The other commercially available conductor made from Nb₃Sn gives a shift of about 3 T upwards at 4.5 K and could be used for such high field magnets. However, Nb₃Sn superconductor is a very brittle material and cannot be used to wind magnet coils. Instead, the coils have to be wound before the heat treatment needed to produce the superconducting state, which requires them to be heated to over 600 degrees for many tens of hours. Whilst this may be reasonable for a small number of specialized magnets, it is clearly not feasible for a large series.

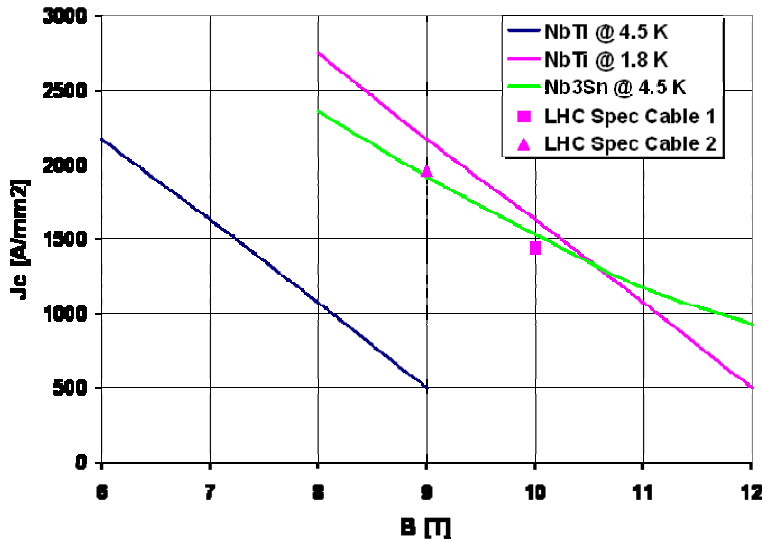


Figure 3: Critical current density of superconductors.

The other way to high fields is to cool conventional superconductor to lower temperature. It can be seen from Figure 3 that Nb-Ti cooled to 1.8 K gives the same 3 T shift as Nb₃Sn. This is a much more economical way to getting the high fields needed. However, it does not come without difficulties. First of all, there is a phase transition in helium at 2.17 K when the liquid becomes superfluid. The advantages and disadvantages of this are discussed below. In addition, the heat capacity of the superconductor decreases by an order of magnitude between 4.5 and 1.8 K, so for a given heat inleak into the cable, for example due to small movement under the very high electromagnetic force or heating due to beam loss, the temperature rise is much higher, making the magnets much more sensitive to quenches. However, the superfluid helium can help if the coils are properly engineered.

A twin aperture dipole consists of two dipoles in a common iron yoke (Figure 4). The two coils are clamped with austenitic steel collars with very low permeability surrounded by a yoke of low carbon steel which carries the magnetic flux. Figure 5 shows the flux plot as computed for the whole structure of the main dipole.

The requirement that the field must be in the opposite directions in the two apertures (for a proton-proton collider) ensures that there is no saturation of the central part of the yoke. The stored energy of 500 kJ/m in the magnet at nominal field requires active quench protection. If a quench is detected, the whole coil is made resistive by firing a capacitor bank into resistive strips (quench heaters) built into the coil. The current is then diverted through a diode until the power supply can be switched off.

The cross section of one quarter of a coil is shown in Figure 6. The coil is wound in two layers in six blocks separated with copper wedges. The geometry of the conductor distribution has been carefully optimized to achieve as pure a dipole field as possible. The optimum geometry, which minimizes the higher harmonics of the field distribution, has been computed using a genetic algorithm. Once the coil geometry has been fixed, then it is very important to keep it constant during the whole series production.

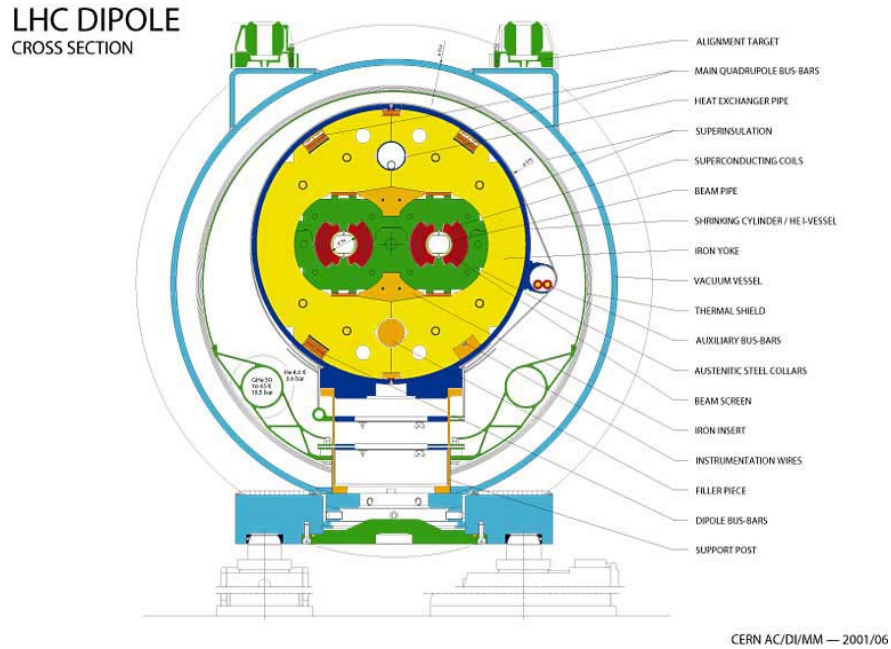


Figure 4: Dipole cross-section.

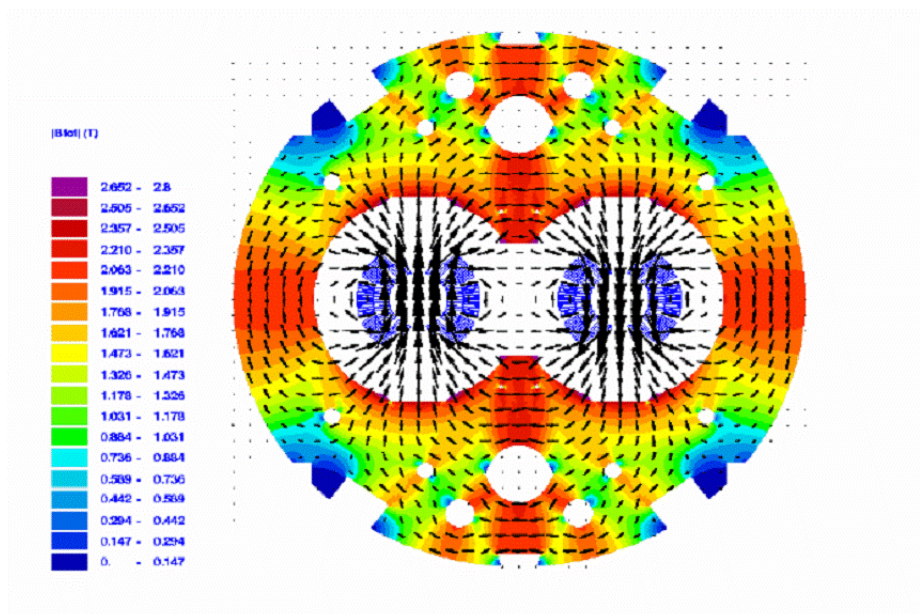


Figure 5: Flux plot in dipole.

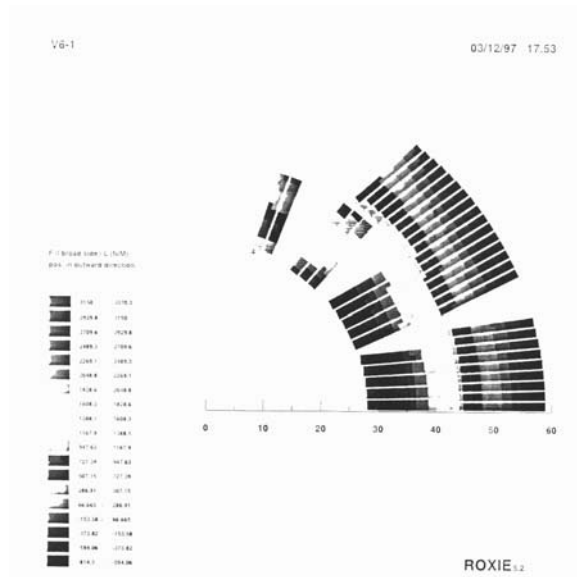


Figure 6: Distribution of conductors in dipole coil. The coil blocks are separated by four copper wedges.

Equipment has been provided to the magnet manufacturers to allow the measurement of the field harmonics in the collared coil before assembly into the yoke. In this way, a tight quality control can be kept throughout the manufacturing run. Figure 7 shows the sextupole component of the field in about 1000 produced magnets. At the beginning of production it was necessary to make two small iterations on the geometry of the copper wedges in order to bring the harmonics inside the required control limits.

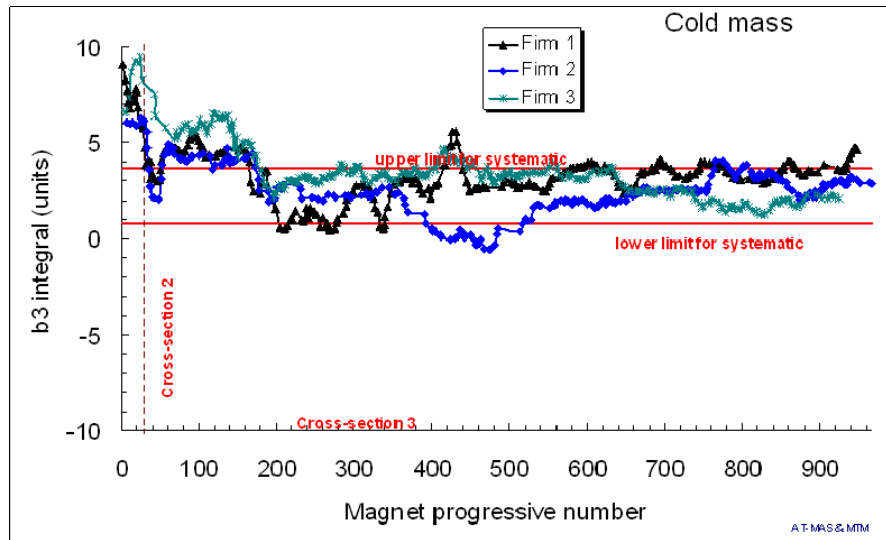


Figure 7: Sextupole component (b_3) of magnetic field in 1000 of the 1232 dipoles.

Apart from the field quality, it is also important to keep the integrated transfer function (effectively the bending angle for a given current) inside tight limits and identical for all three manufacturers. Too large dispersion in bending angle would result in very large orbit distortion which would be difficult to correct and variation in the mean for the three

manufacturers would require that they are sorted into different octants depending on the manufacturer. Figure 8 shows what has been achieved for 1000 dipoles produced. The dispersion is much smaller than specified and the variation in the mean is so small that magnets from the three manufacturers can freely be mixed, simplifying enormously the logistics.

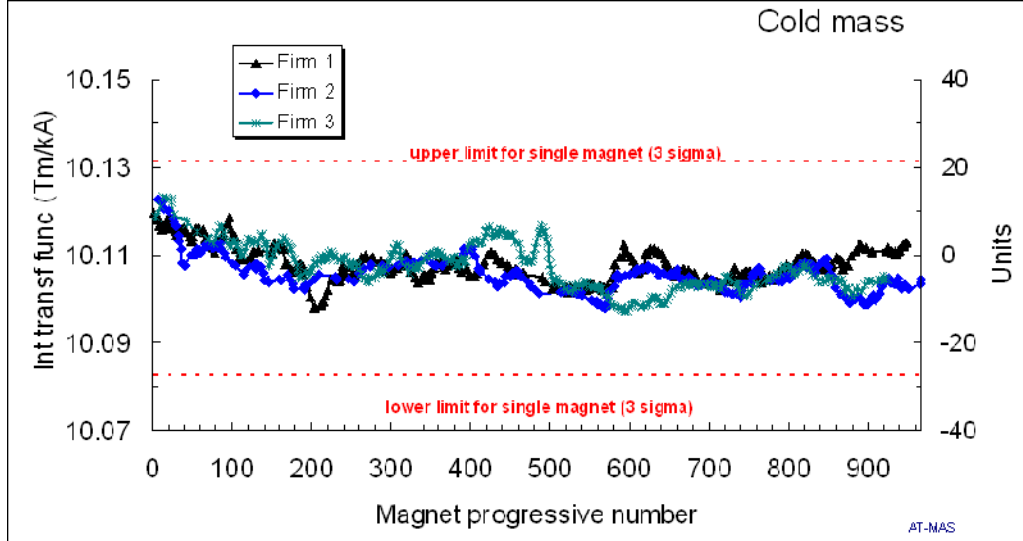


Figure 8: Integrated bending strength measured over 1000 dipoles from three manufacturers.

The main arc quadrupoles, 3.25 m long, are made with the same superconducting cable as the outer layer of the dipoles. Since the electromagnetic forces are much less and the geometry is more suited, the coils have separate austenitic steel collars instead of the combined collar structure of the dipoles. Each quadrupole is integrated into a Short Straight Section (SSS), each containing a sextupole for chromaticity correction and a closed orbit correction dipole. Depending on its position in the arc, a SSS can also contain a trim quadrupole or a Landau octupole.

In addition to the main arc magnets, the LHC contains many more elements for correction of dipole imperfections, matching of the optics and in the final focus. Table 2 gives a full list of all superconducting magnets, their number and function.

Table 2: List of superconducting magnets and their function.

Type	Number	Function
MB	1232	Main dipoles
MQ	392	Arc quadrupoles
MBX/MBR	16	Separation & recombination dipoles
MSCB	376	Combined chromaticity & closed orbit correctors
MCS	2464	Sextupole correctors for persistent currents at injection
MCDO	1232	Octupole/decapole correctors for persistent currents at injection
MO	336	Landau damping octupoles
MQT/MQTL	248	Tuning quadrupoles
MCB	190	Orbit correction dipoles
MQM	86	Dispersion suppressor & matching section quadrupoles
MQY	24	Enlarged-aperture quadrupoles in insertions
MQX	32	Low-beta insertion quadrupoles

2.4. Cryogenics

The LHC magnets are cooled with pressurized superfluid helium, which has some interesting properties that make it a unique engineering material. Best known is its very low bulk viscosity which allows it to permeate the smallest cracks. This is used to advantage in the magnet design by making the coil insulation porous and enabling the fluid to be in contact with the strands of the superconductor. It also has a very large specific heat, 100,000 times that of the superconductor per unit mass and 2000 times per unit volume. Finally the thermal conductivity peaks at 1.9 K (Figure 9) and is approximately 1000 times higher than that of cryogenic grade OFHC copper. The helium in the coil can therefore make up for the very low specific heat of the conductor at this temperature by helping to absorb unwanted thermal loads and transporting them efficiently outside the coil.

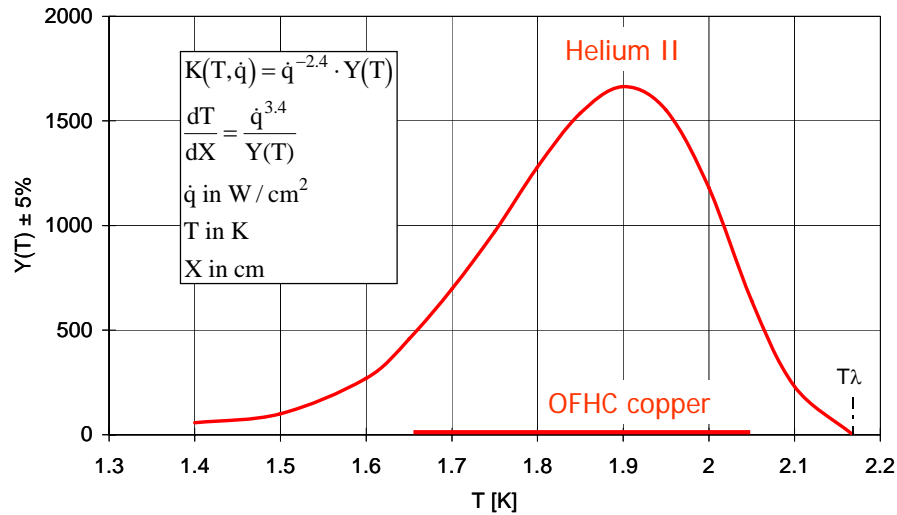


Figure 9: Thermal conductivity of HeII

The most usual method of making superfluid helium in the laboratory is by pumping on the helium bath. Figure 10 shows the phase diagram of helium in the region of the point of the phase transition (the lambda point). Pumping on the bath reduces the pressure and at around 50 mbar and at a temperature of 2.17 K it crosses the lambda point. Further reduction of the pressure to 15 mbar lowers the temperature to 1.9 K.

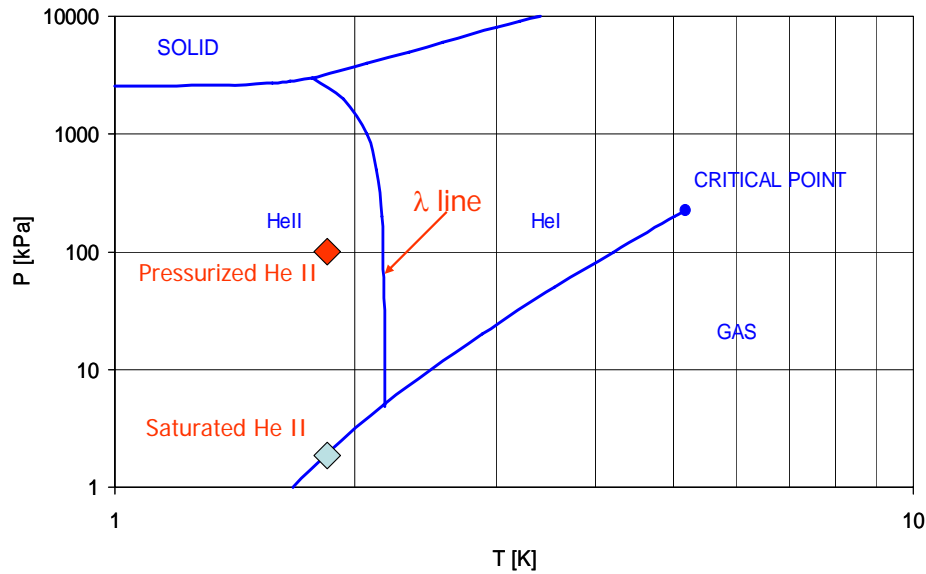
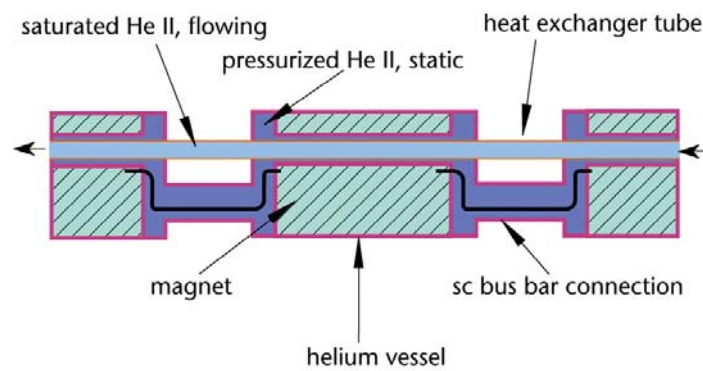


Figure 10: Phase diagram of Helium

The magnets themselves are cooled in a bath of superfluid at atmospheric pressure. This is achieved through a linear heat exchanger traversing each 107 m period of magnets (Figure 11) containing superfluid at 15 mbar pressure, cooling the helium in the magnets at 1 bar to the same temperature as the saturated superfluid inside the heat exchanger. One big advantage of this system is that there is no problem with the bad dielectric strength of gaseous helium since the coil is permanently in liquid.

LHC magnet string cooling scheme



CERN AC - E12-12 VE - V9/9/1997

Figure 11: Linear heat exchanger

The machine is cooled using 8 cryogenic plants, each of 18 kW capacity at 4.5 K, located in pairs at the even points except for one singularity at Point 2. Figure 12 shows the cryogenic architecture at an even point. Four of the refrigerators are recuperated and upgraded from LEP, the other four are new.

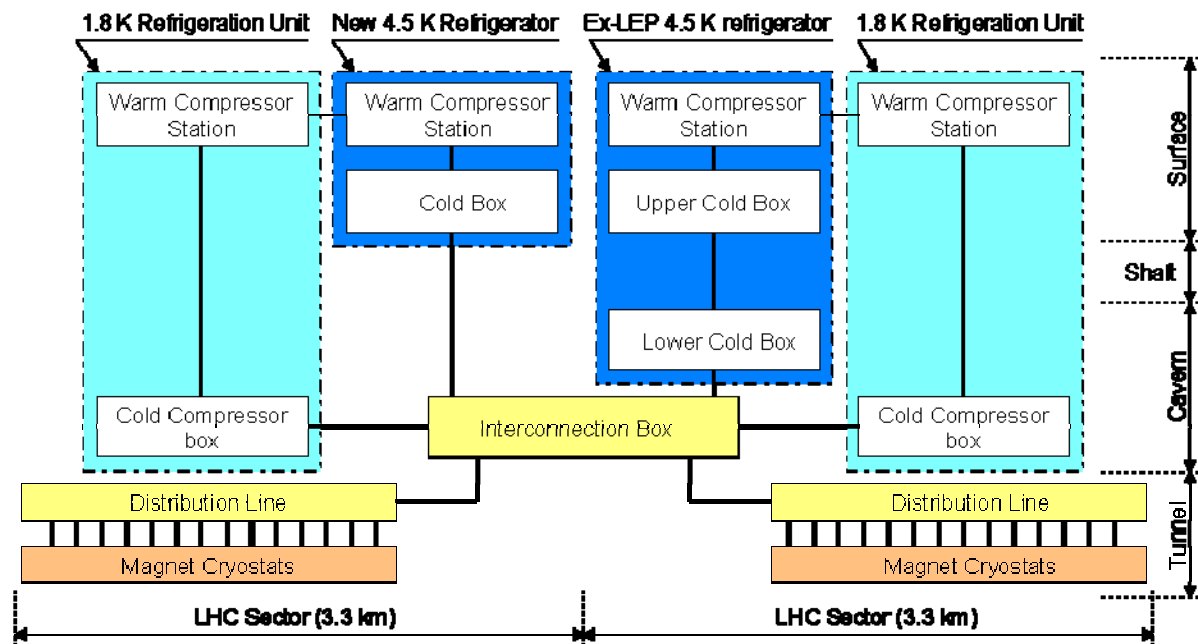


Figure 12: Cryoplant architecture at an even point

The LEP refrigerators have their cold box split between surface and tunnel level whereas the new plants are located on the surface. At the tunnel level, the conventional refrigerators are supplemented by cold compressors. These multi-stage axial centrifugal compressors (Figure 13) pump the cold helium gas, producing the 15 mbar pressure in the linear heat exchangers inside the magnets in order to produce the primary superfluid. The connection to the magnets is made through a cryogenic distribution line running in the tunnel parallel to the machine. An interconnect box allows the plants to be used in the arc either side of the even point or if needed, for the full power of both plants to be used in one arc.

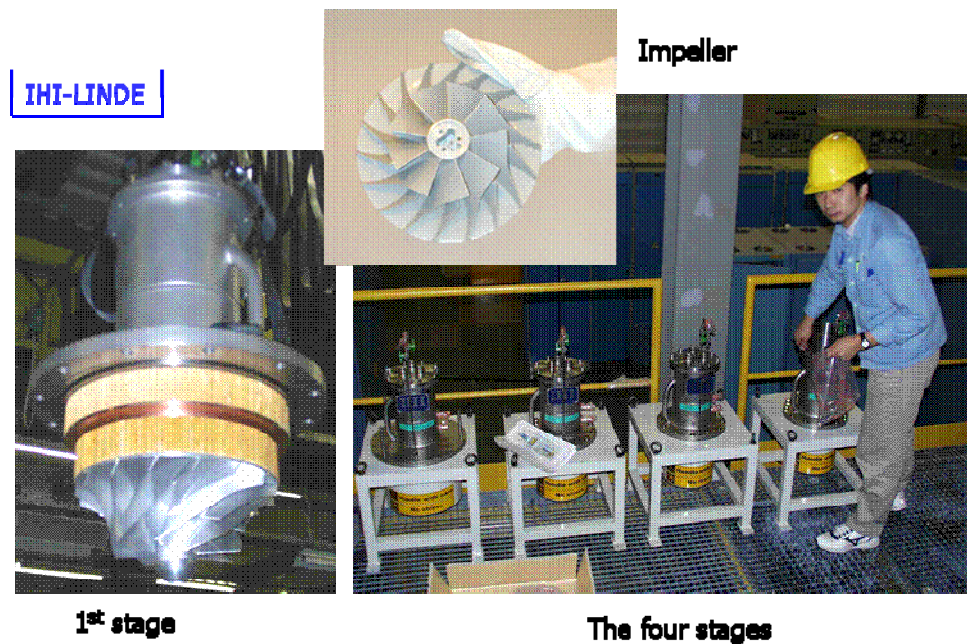


Figure 13: Cold compressor impeller stages.

Using a single cryogenic plant boosted with a liquid nitrogen precooler, a sector can be cooled down in less than 15 days. By coupling two plants to the same octant, this time can be reduced by a factor of two. Warming of a sector takes about the same time.

2.5. The Radiofrequency Acceleration System

The RF system is located at Point 4. Two independent sets of cavities operating at 400 MHz (twice the frequency of the SPS injector) allow independent control of the two beams. The superconducting cavities are made from copper on which a thin film of a few microns of Niobium is sputtered onto the internal surface. In order to allow for the lateral space, the beam separation must be increased from 194 mm in the arcs to 420 mm. In order to combat intrabeam scattering (see below), each RF system must provide 16 MV during coast whilst at injection 8 MV is needed. For each beam there are 8 single cell cavities, each providing 2 MV, with a conservative gradient of 5.5 MV/m. The cavities are grouped into two modules per beam, each containing four cells (Figure 14). Each cavity is driven by an independent RF system, with independent klystron, circulator and load. Although the RF hardware required is much smaller than LEP due to the very small synchrotron radiation power loss, the real challenges are in controlling beam loading and RF noise.



Figure 14: Four-cavity module during assembly

2.6. The Vacuum System

The LHC presents several original requirements compared with classical vacuum systems. It has to ensure adequate beam lifetime in a cryogenic system where heat input to the 1.9 K helium circuit must be minimized and where significant quantities of gas can be condensed on the vacuum chamber. The main heat sources are:

- Synchrotron light radiated by the beam at high energy (0.2 W.M^{-1} per beam, with a critical energy of about 44 eV;
- Image currents (0.2 W.M^{-1} per beam);
- Energy dissipated by the development of electron clouds (see below);
- Energy loss by nuclear scattering (30 mW.M^{-1} per beam).

In order to remove the heat from all these processes but the last with high thermodynamic efficiency, the 1.9 K cold bore of the magnets is shielded with a beam screen cooled to between 5 and 20 K (Figure 15). This beam screen is perforated with about 4% of the surface area to allow the cold bore of the magnets at 1.9 K to act as a distributed cryopump, allowing gas to be condensed on the cold bore surface protected against desorption by bombardment with synchrotron radiation photons.

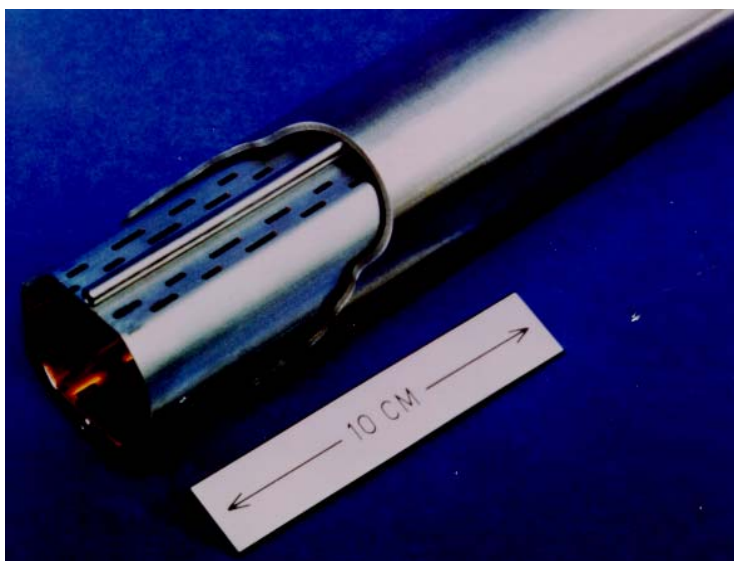


Figure 15: LHC beam screen

For roughly 3 km of the 27 km circumference, mainly in the long straight sections, the vacuum chambers are at room temperature, requiring a low residual pressure without the benefit of the distributed cryopumping. As a spin-off of the development of sputtering technology for superconducting cavities a new getter material (TiZrV) has been developed which can be sputtered on the internal surface of the copper vacuum chambers and can be activated at the very low temperature of 200 degrees (conventional getters require activation at 600 degrees). When activated, the chamber wall itself becomes a distributed pump, producing very low residual pressure and at the same time a very low secondary emission yield, preventing the buildup of an electron cloud. All warm chambers, including those inside the detectors, are treated in this way.

2.7. Accelerator Physics Issues

More than 30 years of accumulated experience from the first hadron collider, the Intersecting Storage rings as well as the proton-antiproton colliders at CERN and FNAL and the superconducting storage rings at BNL and DESY has gone into the LHC design. In the following chapters, the different effects that could limit machine performance and the remedies adopted are described.

2.8. Dynamic Aperture

In superconducting magnets of the type used in the LHC, the field quality is determined by the precision of the positioning of the superconductor and not by the geometry of the iron yoke, so it can never be as good as in conventional magnets. It has been shown by experience in the different superconducting machines and by particle tracking that the aperture inside which particle orbits are stable is much smaller than the physical aperture of the beam pipe. This is called the dynamic aperture and is limited by a complex interplay between the unwanted higher field harmonics due to magnet imperfections. Sophisticated computer codes have been developed to track particle orbits around virtual machines with distributed random and systematic imperfections. And these results are used to define

maximum systematic and random deviations of each field multipole. It was from this work that the control limits for the sextupole component of the dipole field shown in Figure 7 were derived. Even with present day computers it is not possible to perform full scale simulation over a large number of virtual machines over 4×10^7 turns, which corresponds to 1 hour of storage time. The dynamic aperture obtained from tracking of existing machines is always too optimistic when compared to experiment by 20% or more. For the LHC, in order to insure a dynamic aperture of 6 sigmas it has been decided that the tracked dynamic aperture over 10^6 turns should be a factor of 2 larger. These results have been used to supply the tables of allowed multipole errors to the magnet builders.

Since the dynamic aperture depends strongly on the horizontal and vertical tunes, the tracking studies are also used to find the best working points.

2.9. The Beam-Beam Interaction

When the beams are brought into collision, a much stronger nonlinearity than the magnet imperfections comes into play. It is called the beam-beam interaction and is caused by the force due to the electromagnetic field of one beam on the particles in the other beam. It produces two main effects.

The first is to cause a variation of the tune with amplitude. This means that the beam does not occupy a point on the Q_h, Q_v tune diagram but produces an extended “footprint” The second effect is that because of the periodic nature of the force (particles experience a delta function kick on each revolution) it excites nonlinear resonances which can strongly limit the beam lifetime. Figure 16 is an example of a tune scan made many years ago on the SPS proton-antiproton collider. The lower figure shows the tune diagram with nests of 10^{th} , 7^{th} and 11^{th} order resonances. The beams are scanned across these resonances in steps, the lines corresponding to each scan position being intended to indicate approximately the size of the footprint. The upper diagram shows a chart recorder output of the intensity decay of the beams for each position in tune space. In this experiment, the antiproton intensity was very low so that the effect of the beam-beam interaction of the antiprotons on the protons is very small. Consequently, as observed, the decay rate of the protons is completely insensitive to the tune. On the other hand, the strong proton beam affects the antiprotons much more, producing a clear effect as the beams are scanned across the resonances. Experiments like this indicate that the total tune spread due to the sum of the tune spreads from each interaction point should not exceed 0.015. With three proton detectors requiring almost head-on collisions this implies that the tune shift per experiment should not exceed 0.005, a value routinely achieved in previous and existing colliders.

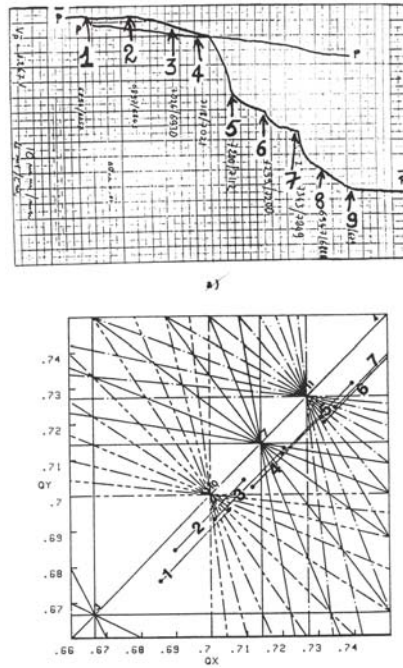


Figure 16: A beam-beam resonance scan at the SPS collider

The long-range beam-beam interaction between successive bunches must also be avoided by colliding the beams with a small crossing angle of about 400 micro radians.

2.10. Intrabeam Scattering

As particles perform their betatron and synchrotron oscillations, they exchange energy due to multiple Coulomb scattering. The correct frame of reference to understand the phenomenon is the rest frame of the beam. The transverse rms momenta $\sigma'_{x,y}$ are unchanged by this transformation whereas the longitudinal momentum σ_p is transformed into σ_p/γ . In a highly relativistic beam like the LHC, the longitudinal plane is therefore very “cold” compared with the transverse planes and one would expect a damping of the transverse dimensions and an increase in the energy spread, which would be good for luminosity preservation. This indeed does occur in the vertical plane although the damping time is very long. Unfortunately, in the regions where the dispersion is not zero (most of the machine), a particle changes its energy by Coulomb scattering but does not change its position and therefore finds itself on the wrong orbit for its momentum. It can only make a betatron oscillation around its new equilibrium orbit, adding a heating term that completely swamps the slow damping in the radial plane.

Intrabeam scattering has been clearly observed in the SPS proton-antiproton collider (Figure 17) and the growth rate is in quite good agreement with the theory. In the LHC, if no action is taken, the beam would blow up so fast that the luminosity lifetime would be reduced to a few hours.

The growth rate depends strongly on the 6-dimensional phase space density. The longitudinal emittance of the beam arriving from the SPS is about 1 eV.s. During the acceleration, the emittance is increased to 2.5 eV.s using RF noise to blow up the energy spread and bunch length. This reduction in phase space density is sufficient to increase the transverse emittance growth time to about 80 hours, making its effect on luminosity lifetime negligible compared to

other processes. A consequence of this is that the RF voltage during coast must be increased to 16 MV to provide a big enough bucket for the large emittance beam.

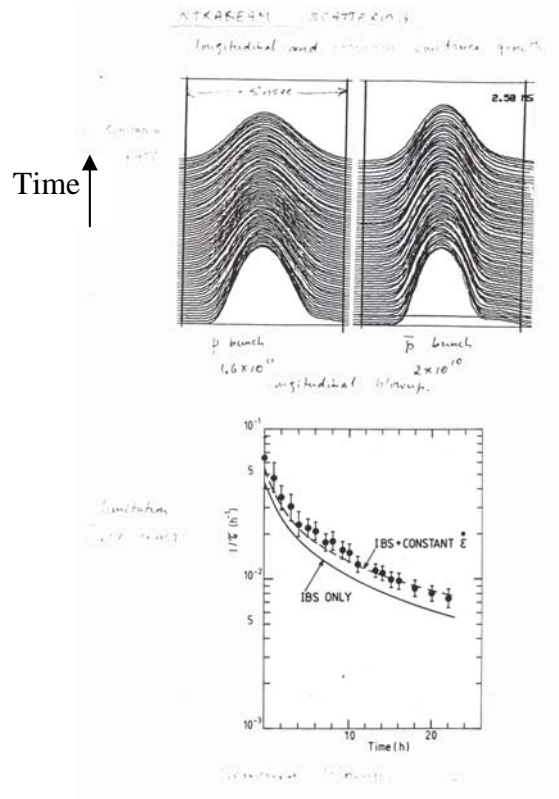


Figure 17: Intrabeam scattering in the SPS. Top Bunch lengthening with time for a strong proton bunch (left) and a weak antiproton bunch (right) Bottom. IBS growth rate compared with theory.

2.11. Coherent Instabilities

The interaction of the beam with its environment generates electromagnetic fields which can react back on it and drive it unstable. The first remedial action is to design the vacuum chamber to reduce this coupling as much as possible. The chamber should be as smooth as possible without discontinuities. As an example, Figure 18 shows an interconnect module between two dipoles. When the magnets are cold, the bellows is stretched and the RF “fingers” ensure a smooth transition from one beam screen to the other. The material of the beam screen is stainless steel to give it structural strength in case of quench co-laminated with a 75 micron layer of copper on its inner surface. The resistivity of the copper layer is reduced by cooling it to between 5 and 20 K. In the room temperature regions the vacuum chamber is made of 2 mm thick high conductivity copper.

Reducing the impedance of the environment can reduce the growth rate of the instabilities but cannot eliminate them all together. In the LHC, the two instabilities that must be controlled are the transverse coupled bunch instability (resistive wall) and the single bunch head-tail instability.



Figure 18: A vacuum interconnect

The resistive wall instability is driven mainly by the long-range wake fields due to image currents in the beam screen. The instability can occur at the frequencies of the so-called slow waves:

$$f_n = (n - Q)f_r$$

where f_r is the revolution frequency (11.245 kHz), Q is the tune and n is the mode number. Only modes with $n > Q$ are unstable. The other modes drive backward waves which are stable.

The lowest and fastest growing mode is around 8 kHz ($Q=59.3$) with a rise time of around 300 turns (26 ms). It must be damped with active feedback. A signal from a transverse pickup is delayed by one turn, amplified and fed back into a pair of electrostatic deflectors placed at a betatron phase of 90 degrees with respect to the pickup. The bandwidth of the system is around 20 MHz, allowing many modes to be damped simultaneously. Very high frequency modes have such slow growth rates that they will be damped by Landau damping (see below). The transverse feedback system is also useful for damping injection errors to avoid filamentation and emittance growth.

The head-tail instability is a well-known single bunch effect driven by short-range wakefields where the tail of the bunch is driven by the head and half a synchrotron period later the roles are reversed, driving the bunch unstable. For the lowest head-tail mode this can only happen if the chromaticity is negative. The chromatic aberrations must anyway be corrected by the sextupoles integrated into the short straight sections. To control the head-tail instability it is sufficient to keep the chromaticity slightly positive at all times. This will be particularly critical at the start of acceleration where persistent currents in the superconducting magnets can produce a large and rapid change in the chromaticity.

The ultimate panacea for beam instabilities is Landau damping where the tune spread in the beam is large enough to stop it from oscillating coherently. To provide Landau damping, two families of strong octupoles are integrated into the lattice in selected short straight sections. Octupoles give a variation of tune with betatron amplitude and will allow instability control at high energy without active feedback. This will be particularly important if the transverse feedback

system has noise problems. During collisions, the tune spread due to the beam-beam footprint should be enough to keep the beams stable.

2.12. Electron Cloud Effects

A significant number of electrons can accumulate in the LHC vacuum chamber through ionization of residual gas molecules or by the impact of synchrotron radiation on the beam screen. When a proton bunch passes, these electrons will be given an impulse and can hit the beam screen with energies of several hundred electron volts. The primary electrons produce secondaries (figure 19) and if the transit time of the electrons across the chamber is resonant with the 25 nsec bunch separation, the electron cloud can grow exponentially. This process is called beam-induced multipacting and is known to limit the performance of storage rings with small bunch separation, notably the two B factories, PEP-II and KEKB.

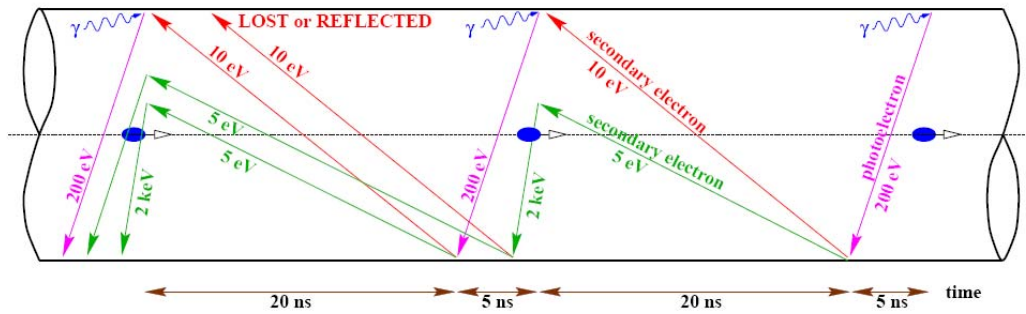


Figure 19: The electron cloud effect

The threshold for the buildup of the electron cloud depends on the bunch current, the geometry of the beam screen and the secondary emission yield (SEY) of the surface of the beam screen. It has been shown that it can occur in the LHC under some conditions with the nominal bunch separation and has already been observed in the SPS with LHC-like beams. The main effect is an additional heat load in the cryogenic system and can also lead to instabilities.

A considerable amount of work has been done in order to understand the phenomenon, both experimentally and through the development of simulation codes which have been calibrated on experimental data from the SPS. Figure 20 shows the predicted heat load on the beam screen as a function of bunch intensity for the nominal 25 nsec bunch separation with different values of the secondary emission yield of the beam screen surface. The available cooling capacity of the cryogenic system is also shown. At zero intensity, all of the capacity is available for the electron cloud but as the intensity increases, part of the capacity is used for image currents and synchrotron radiation. The main conclusions are the following.

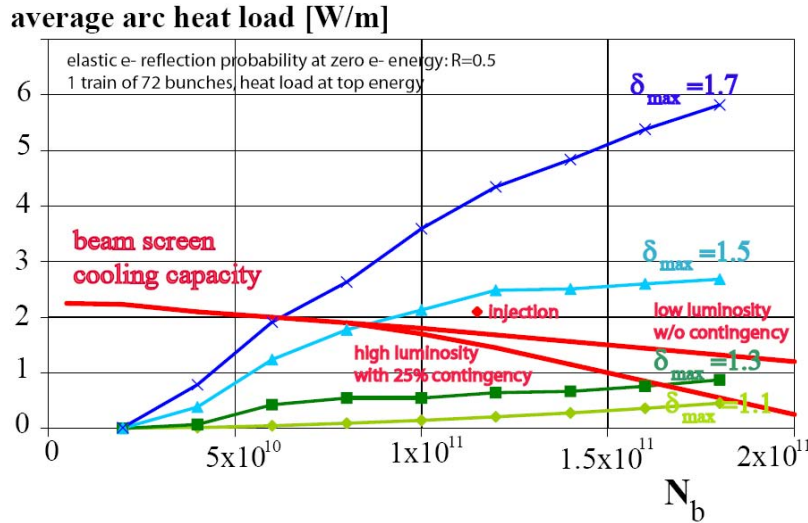


Figure 20: Heat load on the beam screen for different values of SEY.

For the raw surface of the beam screen with a SEY of around 1.7, the electron cloud will limit the intensity to about half nominal. It has been shown experimentally that the presence of the cloud “scrubs” the surface and the SEY reduces quickly to below 1.3, where this effect should no longer be a problem up to and beyond nominal intensity. Simulations also show that for larger bunch separations, above 50 nsec, the threshold is well above nominal intensity. For this reason, the LHC injector chain has been equipped to provide beam a beam of 75 nsec as well as the nominal one, so that early commissioning can be done without the need for a scrubbing run.

3. CONCLUSIONS

The LHC is now in its final stage of installation and commissioning. A beam has already been extracted from the SPS with the parameters needed to achieve design luminosity and has been transported along the 2.6 km tunnel TI8 to the LHC injection point. The stored energy in this beam at 7 TeV is two orders of magnitude higher than in any previous machine and one of the biggest challenges will be to ensure that the machine protection systems work with an extremely high degree of reliability in order to protect both machine and detectors.

The accelerator physics is well understood and the appropriate means to combat the various effects have been integrated into the machine design. The one new effect not seen in hadron machines before is the electron cloud. Simulations and experiments on the SPS have shown that a moderate scrubbing of the surface of the beam screen by electron bombardment will quickly reduce the secondary emission yield to a low enough value to allow design luminosity to be reached.

References

- [1] LHC Design Report, CERN-2004-03, (2004).